Geomechanics and Engineering, *Vol. 20, No. 4 (2020) 359-370*
DOI: https://doi.org/10.12989/gae.2020.20.4.359

Prediction of the load-displacement response of ground anchors via the load-transfer method

Juraj Chalmovský* and Lumír Mička[a]

Department of Geotechnics, Faculty of Civil Engineering, Brno University of Technology, Veveri 331/95, 602 00 Brno, Czech Republic

(Received August 27, 2019, Revised January 7, 2020, Accepted February 4, 2020)

Abstract. Prestressed ground anchors are important structural elements in geotechnical engineering. Despite their widespread usage, the design process is often significantly simplified. One of the major drawbacks of commonly used design methods is the assumption that skin friction is mobilized uniformly along an anchor's fixed length, one consequence of which is that a progressive failure phenomenon is neglected. The following paper introduces an alternative design approach – a computer algorithm employing the load-transfer method. The method is modified for the analysis of anchors and combined with a procedure for the derivation of load-transfer functions based on commonly available laboratory tests. The load-transfer function is divided into a pre-failure (hardening) and a post-failure (softening) segment. In this way, an aspect of non-linear stress-strain soil behavior is incorporated into the algorithm. The influence of post-grouting in terms of radial stress update, diameter enlargement, and grout consolidation is included. The axial stiffness of the anchor body is not held constant. Instead, it gradually decreases as a direct consequence of tensile cracks spreading in the grout material. An analysis of the program's operation is performed via a series of parametric studies in which the influence of governing parameters is investigated. Finally, two case studies concerning three investigation anchor load tests are presented.

Keywords: ground anchor; pullout capacity; load-transfer method; progressive failure; grout

1. Introduction

Ground anchors are frequently used to stabilize retaining structures, deep cuts, landslides, foundations against uplift, etc. Recommendations for design, execution, and testing of prestressed ground anchors might be found in the following standards: EN 1997-1 (2004), EN 1537 (2013) and ISO 22477-5 (2018). It is possible to distinguish two groups of design methods commonly used to determine the load-bearing capacity of these elements. The first one consists of semi-empirical methods (Littlejohn (1980), Barley (1997), Krammer (1978) and others). These methods take the form of closed-form expressions. Thus, dimensional variables and soil properties are directly involved in the design process. One or multiple empirical constants are incorporated into the expressions. The second group contains various empirical methods (Ostermayer (1975), Misove (1984), PTI (2004) and others) which are available in the form of tables and graphs with recommended skin friction values and carrying capacities for representative types of soils.

These procedures are reliable but are mostly intended only for specific geological conditions. The wide ranges of recommended values are the result of necessary generalization with respect to predefined soil types. The non-uniformity of shear stress distribution and progressive failure cannot be quantified directly. The effect of post-grouting is considered either via empirical constants or by separate recommended skin friction values. Furthermore, the standard design process output is mostly only the ultimate carrying capacity with no additional information about the displacements required in order to mobilize it, or about stress, force and displacement distributions along the fixed length for different loading stages.

The paper presents an alternative ground anchor design approach for cohesive soils employing the load-transfer method (Reddy *et al.* (1998)). This method is slightly modified and combined with a procedure for the derivation of load-transfer functions based on commercially available laboratory tests (Kraft *et al.* (1981)). The factors of non-uniform shear stress distribution, post-grouting, and limited grout tensile strength are included in the algorithm. The primary calculation outcome is a load-displacement curve. Furthermore, shear stress, axial force and displacement distributions along the fixed length are obtained for each loading stage. After a theoretical description of the principles involved in the algorithm, the influence of governing parameters is analyzed by a series of parametric studies. Finally, two case studies concerning three investigation anchor load tests are presented. The tested anchors were equipped with electric resistance gauges, making it possible to derive profiles of mobilized shear stress and compare them with predictions.

2. Factors influencing the load-displacement behavior of ground anchors

In this section, factors significantly influencing the

*Corresponding author, Ph.D.
E-mail: chalmovsky.j@fce.vutbr.cz
[a]Associate Professor

Copyright © 2020 Techno-Press, Ltd.

ISSN: 2005-307X (Print), 2092-6219 (Online)

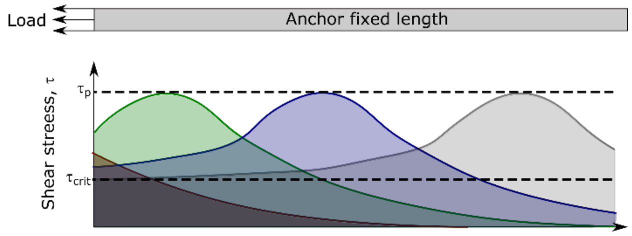

Fig. 1 Non-uniform shear stress distribution along anchor fixed length

performance of prestressed ground anchors in cohesive soils are briefly introduced. These aspects are consequently included in the developed algorithm.

2.1 Non-uniform shear stress mobilization and progressive failure

The mobilization of shear stress along the fixed length of ground anchors is non-uniform during anchor loading. In the first loading stages, mobilized shear stresses at the grout-soil interface are concentrated at the top of the fixed anchor length. After reaching the peak shear strength τ_p, shear stresses gradually drop towards the critical value τ_{crit} and the peak bond strength location moves along the fixed anchor length, as is schematically shown in Fig. 1. The non-constant (peak) shear stress distribution along axially loaded members such as anchors and piles has been studied by several authors e.g. Ostermayer (1975), Barley (1997), Wu *et al.* (2015), Vukotic *et al.* (2013).

Based on the regression analysis of anchor loading tests performed mainly in very stiff clays, Barley (1997) has proposed a closed-form formula for the efficiency factor f_{eff} (Eq. (1)) and for the ultimate carrying capacity of low pressure grouted anchors F_{ult} (Eq. (2)), where L_{fixed} is the fixed anchor length, D is the borehole diameter and s_u is the undrained shear strength. The progressive failure mechanism is an important factor in the case of anchors constructed in stiff to very stiff cohesive soils and dense to very dense non-cohesive soils exhibiting peak shear strength. This strength is reduced during strain softening towards a critical stress state. Woods and Barkhordari (1997) proposed another empirical formula for the efficiency factor appropriate for non-cohesive soils.

$$f_{eff} = 1{,}6 L_{fixed}^{-0{,}57} \tag{1}$$

$$F_{ult} = \pi D L_{fixed} f_{eff} s_u \tag{2}$$

2.2 Post-grouting

Post-grouting significantly affects the load-displacement response of ground anchors and piles. The post-grouting effect has been experimentally analysed by Ostermayer (1975), Bustamante and Diox (1985), Larsen (2007), Mothersille *et al.* (2015), Zou *et al.* (2019) and others. Experimental evidence suggests that the ultimate carrying capacity increases with rising grouting pressure and volume of injected grout. At some point, however, the effect of these two factors begins to diminish, which is probably due to the occurrence of soil cracks via which the grout can flow away from the fixed length. The ultimate carrying capacity also increases if grout injections are performed in multiple stages. The effect of post-grouting can be divided into two parts:

- Enlargement of the fixed length diameter.
- An increase in the radial stresses acting on the fixed length surface and consequently the shear strength of the grout-soil interface.

2.3 The limited tensile strength of grout and the occurrence of tensile cracks

The prestressing force is transferred to the surrounding soil by the tendon-grout and grout-soil interface. The grout material is thus loaded by tension. At a certain axial strain level, tensile cracks start to occur. Weerasinghe and Littlejohn (1997) performed a series of tests on full-scale laboratory models. After the model anchors were loaded, radial cracks with distances between 20 and 220 mm were observed in the grout surrounding the tendon along the fixed length. The occurrence of tensile cracks in the grout material and their gradual spreading was observed during continuous strain measurement with a fiber optic system (Monsberger *et al.* (2017)) and further simulated (Fabris *et al.* (2018)) via the finite element method. Tensile crack formation reduces overall anchor axial stiffness and thus affects the load-displacement curve shape and the uniformity of shear stress distribution.

3. Theoretical principles

The factors described above are often not explicitly included in the design process. The procedures and principles necessary for their incorporation and quantification are specified in this section. First, the load-transfer method is introduced together with a procedure for the determination of a load transfer function shape. The calculation of the compound stiffness of the anchor cross-section is then explained. Rules governing the gradual decrease in this stiffness due to the occurrence of tensile cracks are specified afterwards. Finally, the incorporation of the post-grouting factor via a version of the cavity expansion theory is described.

3.1 The load-transfer method and load-transfer functions

The load-transfer method (*t-z* method) is based on the idea that an axially loaded member (e.g., a tension or compression pile) can be divided into a finite number of segments to which the unique dependence between the segment vertical displacement (z) and the shear stress mobilized on its surface (τ) is assigned. The τ–z function is called the load-transfer function. A similar function for normal stress (σ–z) is added for the pile tip in the case of compression piles. The *t-z* method was originally developed for prediction of the load-displacement response of axially loaded piles. An extensive database of applications for both driven and bored piles can be found in Bohn *et al.* (2017). Several modifications of the original procedure for various types of constructions have been derived such as piles subjected to loading-unloading cycles (Dias and Bezuijen (2017)), rectangular closed diaphragm walls (Wu *et al.* (2016)) and pile groups (Zhang *et al.* (2014)). In order to derive the load-transfer function shape experimentally, it is necessary to perform an instrumented load test up to failure including strain measurements at multiple depths. Pelecanos and Soga (2018) recently obtained non-linear load transfer curves for axially loaded piles from distributed fibre optic sensing and similar curves were applied also for ground anchors (Seo and Pelecanos (2018)).

Conducting a full-scale load test, however, might be economically and time-demanding. Thus, another approach proposed by Kraft *et al.* (1981) in which the theoretical load-transfer function is constructed based on standard laboratory tests is followed. The *t-z* curve is divided into two segments (Fig. 2):

- The pre-failure segment: mobilized shear stress is increasing towards its peak value.
- The post-failure segment: mobilized shear stress is decreasing towards the critical state.

The vertical displacement z of each anchor segment during hardening is governed by Eq. (3), where τ_0 is the shear stress mobilized on the segment surface with the radius of r_0, τ_p is the peak bond strength, R_f is the stress-strain curve-fitting constant, G_i is the initial shear modulus and r_m is the radius of the zone influenced by anchor loading. The concentric cylinder approach proposed by Randolph and Wroth (1978) is combined with a non-linear (hyperbolic) expression of soil stress-strain behavior in this equation.

$$z_s = \frac{\tau_0 r_0}{G_i} ln \frac{\frac{r_m}{r_0} - \frac{\tau_0 R_f}{\tau_p}}{1 - \frac{\tau_0 R_f}{\tau_p}} \tag{3}$$

Despite the fact that the approach of Randolph and Wroth (1978) was originally developed for axially loaded piles, its key assumptions are also relevant for ground anchors: (1) soil displacements around an anchor can be approximated as concentric cylinders; (2) radial displacements are negligible compared to axial displacements; (3) mobilized shear stress decreases with radial direction in such a manner that $\tau r = \tau_0 r_0$; (4) displacements due to anchor loading are negligible beyond the zone of influence with the radius of r_m. The initial shear modulus G_i is determined from the theory of elasticity by Young's modulus E_i and Poisson's ratio τ'. The stress-stiffness dependency is further incorporated according to Duncan and Chang (1970) (Eq. (4)), where p_a is the atmospheric pressure, K is the modulus number and n is the modulus exponent.

$$G_i = \frac{K p_a \left(\frac{\sigma'_3}{p_a}\right)^n}{2(1+\nu')} \tag{4}$$

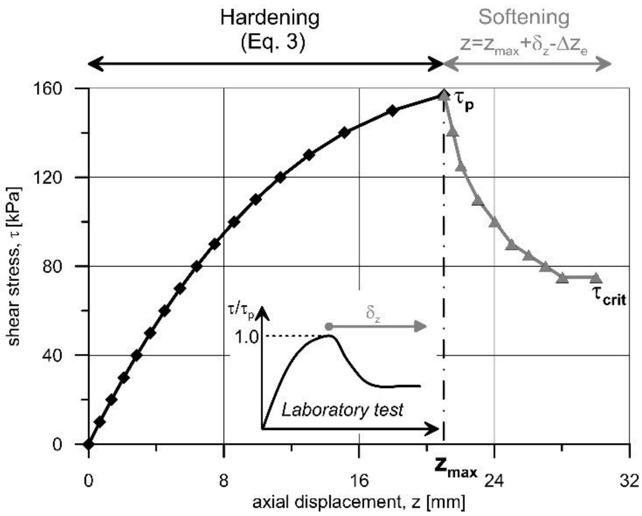

Fig. 2 Load-transfer function proposed by Kraft *et al.* (1981)

The Mohr-Coulomb failure criterion (Eq. (5)) is used to obtain the peak bond strength, where c_p is the peak cohesion, ϕ_p is the peak angle of internal friction and σ'_{rad} is the effective radial stress acting on the surface of the anchor's fixed length. It must be noted that due to the non-linearity of the peak strength envelope, the peak shear strength characteristics c_p, ϕ_p must be chosen with regard to the range of radial stresses acting on the fixed length surface.

$$\tau_p = c_p + \sigma'_{rad} tan\phi_p \tag{5}$$

It is not possible to apply Eq. (3) to the post-failure segment of the load-transfer function due to the development of slip surfaces directly on the fixed length surface (the grout-soil interface) or in its vicinity (the soil-soil interface). Kraft *et al.* (1981) proposed constructing the post-failure segment of the load-transfer function using the direct shear test. Displacements δ_z measured during laboratory tests (Fig. 2) are adjusted by the elastic rebound Δz_e (snap-back) occurring in the soil beyond the slip surface due to unloading in the post-failure regime (Eq. (6)). Corrected displacements Δz and corresponding values of shear stress are then used in the load-transfer functions.

$$\Delta z = \delta_z - \Delta z_e \tag{6}$$

It must be noted that this procedure has several drawbacks: (1) the occurrence of stress concentrations, the influence of boundaries and the small contact area in laboratory experiments; (2) constant normal stress during laboratory tests; (3) the influence of test type. On the other hand, the investigation anchor load tests of anchors with reasonable fixed lengths (8 to 12 m) and simulations adopting the finite element method in combination with a constitutive model which includes strain softening performed by the authors both revealed a rapid failure mode with a fast drop in prestressing force to the stable critical level. From this point of view, it is more important to determine the critical shear strength than the rate of softening towards it. Measured post-failure segments were approximated by a piecewise linear function in this study.

3.2 Ideal cross section, equivalent stiffness

The ideal cross-sectional area A_i of the fixed length consisting of the grout (cross-sectional area A_g) and the tendon (cross-sectional area A_s) is determined according to Eq. (7), where α is the tendon-grout stiffness ratio (Eq. (8)). In order to maintain the real dimensions of the anchors fixed length (the cross-sectional area A_{real}), the equivalent modulus of elasticity E_{eq} is derived according to Eq. (9). Contrary to previous applications of the load-transfer method, the axial stiffness is not held constant throughout the calculation. It gradually decreases as the fixed length is weakened by tensile cracks.

$$A_i = A_g + \alpha A_s \tag{7}$$

$$\alpha = E_s / E_g \tag{8}$$

$$E_{eq} = \frac{E_g A_i}{A_{real}} \tag{9}$$

3.3 Tension stiffening of tendon-grout system

In order to predict anchor head displacements during loading more correctly, it is necessary to take into account the gradual decrease in the axial stiffness of the tendon-grout system due to the occurrence of tensile cracks in the grout. This mechanism is similar to the tension stiffening of a concrete beam with centrally placed reinforcement. A schematic load-displacement curve for such a beam is shown in Fig. 3.

During the initial stages of loading, both the tendon and the grout contribute to the overall axial stiffness EA_{uc}. After reaching the critical force F_{cr} corresponding to the strain ε_{cr}, tensile cracks start to develop and the stiffness contribution of the grout material gradually decreases. The overall axial stiffness approaches the tendon stiffness EA_{cr}. The proposed procedure offers three possible alternatives after grout tensile strength is reached. The most simple of these is to instantly neglect the grout stiffness after the axial strain limit corresponding to the grout tensile strength is reached. Alternatively, the analytical formulations of tension stiffening stated in the CEB-FIP Model Code 1990 (1993) and ACI 318 (2014) are incorporated in the application. The first approach is based on the gradual modification of the effective modulus of elasticity E_{sm} of steel (Eq. (10)), where f_{scr} is the steel stress when the critical force F_{cr} is reached, f_s is the current steel stress state and k = 1.0 for the first loading.

$$E_{sm} = \frac{E_s}{1 - k\left(\frac{f_{scr}}{f_s}\right)^2} \tag{10}$$

The second approach (Eq. (11)) is based on keeping the modulus of elasticity unchanged and subsequently reducing the effective cross-sectional area A_{eff} from its initial intact ideal cross-sectional area (A_i) towards the state where only the tendon area (A_{fin}) contributes to the load transfer. This approach is analogous to the effective moment of inertia concept involved in ACI 318 (2014).

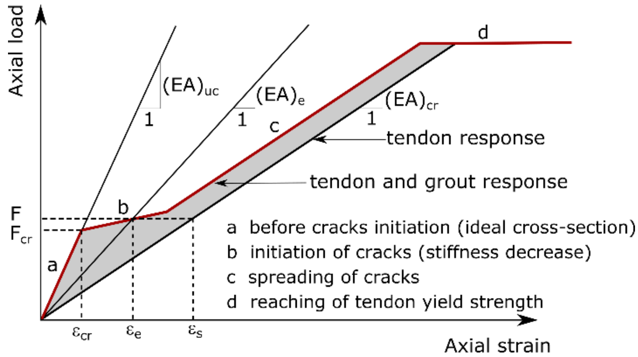

Fig. 3 Idealized axial load-axial strain diagram (after Navratil (2008), modified)

$$A_{eff} = A_i\left(\frac{F_{cr}}{F}\right)^3 + A_{fin}\left[1 - \left(\frac{F_{cr}}{F}\right)^3\right] \tag{11}$$

3.4 Post-grouting

The body of the fixed length is idealized as a cylinder. The incorporation of the post-grouting effect is then divided into three parts. First, the fixed length diameter is calculated based on the effective grout consumption V_i per one manchette valve and the number of valves n_i per 1 m. Secondly, the radial stress increase acting on the fixed length surface is estimated based on the theory of cylindrical cavity expansion. Radial stresses are determined assuming full dissipation of excess pore pressures generated due to the volumetric expansion of the cylindrical body. Based on the finite element analysis, Randolph *et al.* (1979) recommended Eq. (12) for the calculation of the effective radial stress σ'_{rad}, where M is the stress ratio q/p' in triaxial compression (Eq. (13)) and ϕ_{cs} is the critical state angle of internal friction.

$$\sigma'_{rad} = \left(\frac{\sqrt{3}}{M} + 3\right) s_u \tag{12}$$

$$M = \frac{6 sin\phi_{cs}}{3 - sin\phi_{cs}} \tag{13}$$

Finally, in order to estimate the acting radial stress more precisely, grout consolidation is considered. Grout consolidation (bleeding) is a process during which excess water is expelled from the grout, lowering the w/c ratio and the total volume of the grout body. According to Bezuijen and Talmon (2006), the process of grout bleeding will result in a volume loss of between 5 to 10%. Littlejohn (1980), based on multiple anchor loading tests, came to the conclusion that consideration of the full grouting pressure p_i during anchor design may lead to the overestimation of carrying capacity. He recommended the final (residual) pressure $p_{i,res}$ transferred to the soil to be in a range between $1/3p_i$ and $2/3p_i$. The reduction of the effective radial stress $\Delta\sigma'_{rad}$ is calculated according to Eq. (14) (assuming elastic behavior in unloading), where Δr_{fixed} is the fixed length radius decrease due to the grout consolidation.

$$\Delta\sigma'_{rad} = 2G\frac{\Delta r_{fixed}}{r_{fixed}} \tag{14}$$

4. Algorithmization

The developed algorithm is based on the computer routines proposed by Sulaiman and Coyle (1976) and further improved by Reddy *et al.* (1997) and Reddy *et al.* (1998). These routines were developed in order to predict the load-displacement behavior of tension piles while accommodating the load-transfer method. The following changes and improvements to the latest model (Reddy *et al.* (1998)) were performed:

• Assembly of the load-transfer functions based on standard (engineering) soil properties and laboratory tests according to the procedure described in section 3.1.

• Both the tendon and the grout are considered in the calculation of the initial compound stiffness (section 3.2). In contrast with the original procedure, the axial stiffness is not held constant during loading. The rate of decrease is driven by two optional tension stiffening approaches (section 3.3).

• Prior to the calculation of the load-displacement curve, radial stresses acting on the fixed length surface are modified according to section 3.4 in order to take the post-grouting effect into account.

• The initial stiffness Newton-Raphson method is utilized as the load stepping schema.

A flowchart of the application is presented in Fig. 4. During the initial part of the application, the anchor fixed length is divided into a prescribed number of segments. The geometrical characteristics (the coordinates of the end and middle points) are then stored in separate external files. The load-transfer function consisting of a hardening and a softening part is then compiled and assigned to the middle points of each segment. A common load-transfer function is assigned to all segments in the particular stratum. The calculation core, as in the routine developed by Reddy *et al.* (1998), consists of two iteration cycles:

• The inner iteration cycle. Upward deformations of each segment are calculated here. The deformation of each segment is related to its middle point. After the initial assessment of the first segment deformation (assuming zero skin friction acting on its surface), the skin friction is revised and the total shear force acting on the segment surface is determined. The acting shear force leads to a change in the axial force and thus to a segment displacement update. This process is repeated until the prescribed match Tol_{it-1} is obtained in two successive iterations u^x_k and u^{x-1}_k (Eq. (15)), where k is the segment number and x is the iteration number. The inner iteration cycle progresses for each segment. The stress state in the anchor body is also checked at this stage. If the stress state is higher than the grout tensile strength, axial stiffness is modified as described in Section 3.3.

$$|u_k^x - u_k^{x-1}| \le Tol_{it-1} \tag{15}$$

• The outer iteration cycle. After finishing the inner iteration cycle for all segments at the particular loading stage n, the corresponding shear forces $S^n{}_k$ are summed and compared with the external load $F^n{}_{ext}$ (Eq. (16)). If the accuracy condition is not reached, the anchor head displacement is modified and the whole process is repeated.

$$\left| F^n_{ext} - \sum_{k=1}^{n_{seq}} S^n_k \right| \le Tol_{it-2} \tag{16}$$

5. Evaluation and verification of the algorithm

5.1 Influence of governing parameters

The influence of governing parameters on assembled load-transfer functions, predicted load (F) - displacement (u) curves and shear stress distributions along the fixed length is evaluated. The input parameter values for parametric studies were taken from the 1st case study presented in Chapter 5.2.1 and are summarized in Table 1.

The anchor's fixed length was located in overconsolidated stiff clay with high plasticity. The anchor′s free length L_{free} and fixed length L_{fixed} were both 8 m long.

5.1.1 Peak angle of internal friction

Three different values of ϕ_p were utilized. The assembled load-transfer functions are shown in Fig. 5(a). The ϕ_p increase will result in an increase in the peak shaft friction and thus the overall carrying capacity (Fig. 5(b)).

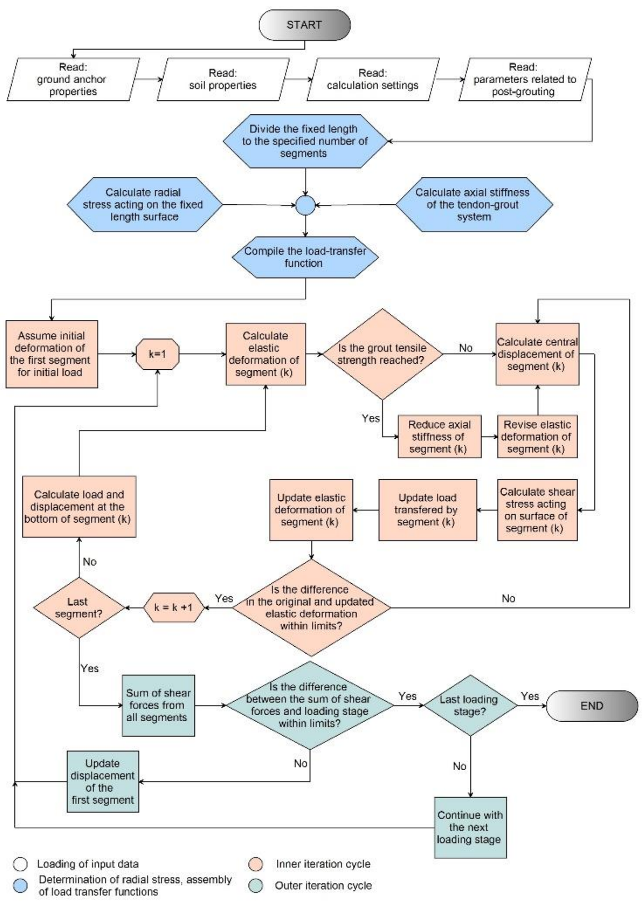

Fig. 4 Flowchart of the proposed algorithm

Table 1 Input parameters values used in parametric studies

Group	Parameter	Symbol	Value
Soil	Angle of internal friction at critical state	ϕ_{cs}	19.9°
	Angle of internal friction at peak state	ϕ_p	14°
	Cohesion at peak state	c_p	90 kPa
	Undrained shear strength	s_u	100 kPa
	Parameters defining stress-stiffness dependence	K	100
		n	0.35
Grout	Fixed length diameter	d_{fixed}	262 mm
	Grout consumption	V_i	17.5 l/valve
	Number of grouting valves per 1m	n_i	2
	Volume loss due to grout bleeding	$\varepsilon_{V,bleed}$	10%
	Tension stiffening approach	-	ACI318
	Grout tensile strength	f_t	2 MPa
Settings	Number of segments	n_{seq}	10
	Toleration of the inner iteration cycle	Tol_1	0.01 mm
	Toleration of the outer iteration cycle	Tol_2	20 kN
	Zone of influence	r_m	2.0 m

Note: Cohesion intercept at critical state is zero

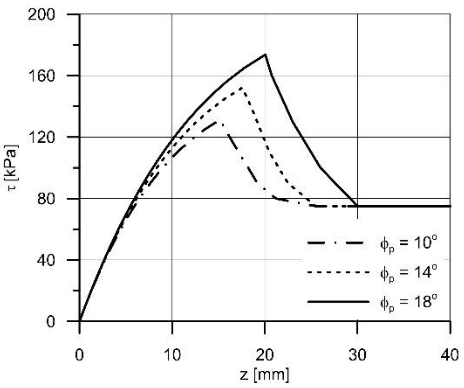

(a) Assembled load-transfer functions

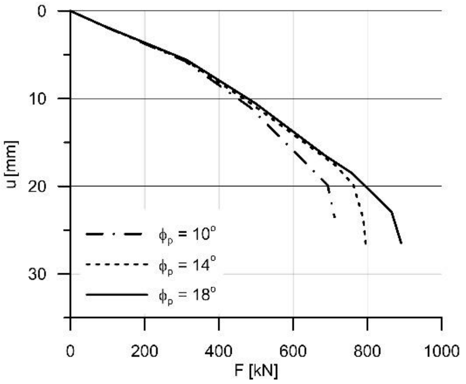

(b) Predicted load-displacement curves

Fig. 5 Influence of peak friction angle

5.1.2 Undrained shear strength

Modification of undrained shear strength s_u results in a change in the radial stress acting on the anchor´s fixed length surface during its expansion due to post-grouting. These aspects are directly incorporated into the load-transfer functions assembly procedure (Fig. 6(a)). The predicted load-displacement curves are shown in Fig. 6(b).

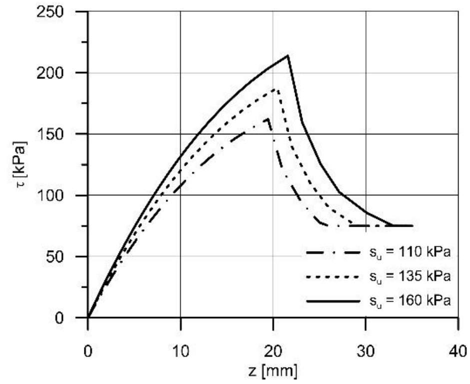

(a) Assembled load-transfer functions

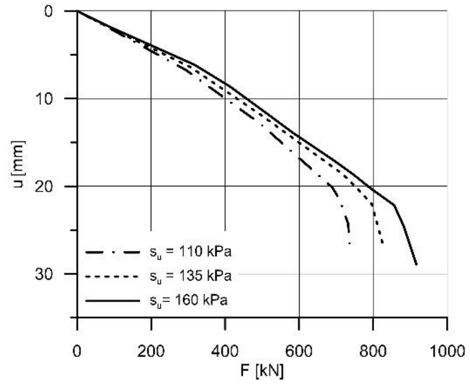

(b) Predicted load-displacement curves

Fig. 6 Influence of undrained shear strength

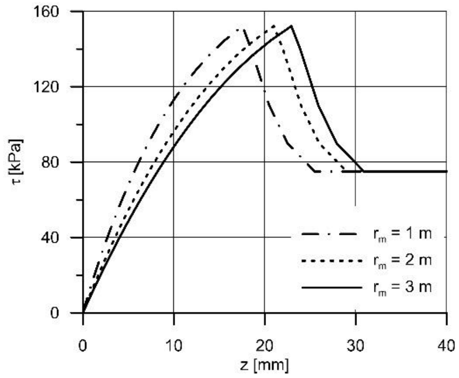

(a) Assembled load-transfer functions

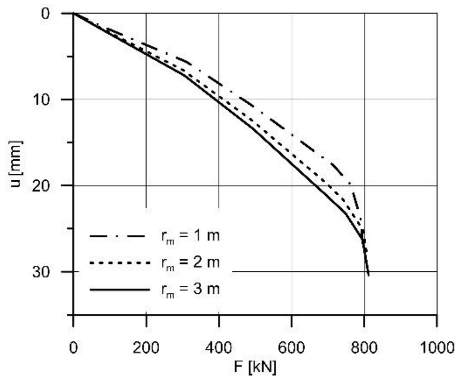

(b) Predicted load-displacement curves

Fig. 7 Influence of radius of zone affected by loading

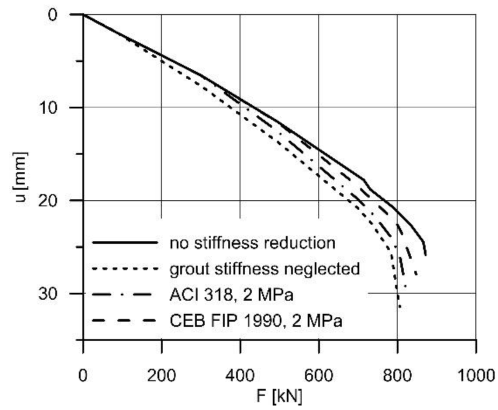

(a) Predicted load-displacement curves

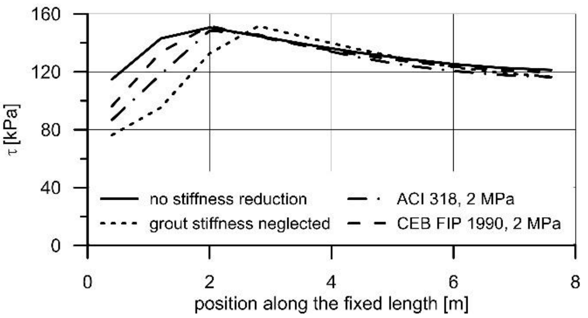

(b) Shear stress distributions

Fig. 8 Influence of grout stiffness and its change

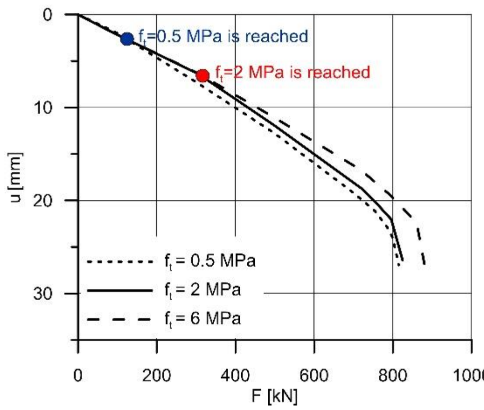

(a) Predicted load-displacement curves

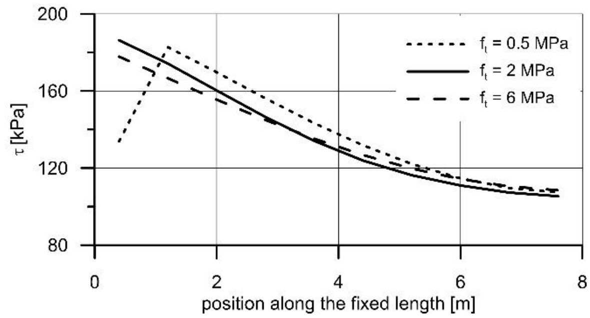

(b) Shear stress distributions

Fig. 9 Influence of grout tensile strength

5.1.3 Radius of the zone affected by anchor loading

Three radii of the zone influenced by anchor loading r_m were used in this analysis. The assembled load-transfer functions and predicted load-displacement curves are shown in Fig. 7(a) and Fig. 7(b) respectively. Change in the r_m parameter results in a stiffness change. The ultimate skin friction and thus the carrying capacity is not influenced.

5.1.4 Grout stiffness and its reduction

Four cases were evaluated in this study:

• No grout stiffness reduction due to the occurrence of tensile cracks. The axial stiffness is held constant during the calculation.

• The grout stiffness (f_t = 0 MPa) is completely neglected.

• Gradual decrease in stiffness according to ACI 318 (2014).

• Gradual decrease in stiffness according to CEB-FIP Model Code 1990 (1993).

In the last two cases, the tensile grout strength f_t = 2 MPa was considered to be initial. The predicted load-displacement curves and shear stress distributions for the ultimate load level are shown in Fig. 8(a) and Fig. 8(b).

Grout stiffness and changes to it do not influence the shape of load-transfer functions. However, it does influence predicted displacements and consequently shear stress distributions. It is evident from Fig. 8(a) that completely neglecting the grout stiffness leads to the lowest overall axial stiffness. In contrast, the alternative which considers grout to be an elastic material leads to the highest axial stiffness value. The alternatives that consider a gradual decrease in stiffness lie between the two previously mentioned extremes. These two alternatives start to deviate from the full line at the point where the grout tensile strength is reached. A decrease in the member axial stiffness leads to a higher degree of non-uniformity in shear stress distributions. Rapid strain softening is triggered on the larger part of the fixed length, resulting in lower ultimate bearing capacity.

5.1.5 Grout tensile strength

Three grout tensile strength values f_t were considered. A gradual decrease in stiffness according to ACI 318 (2014) was applied in all three cases. The predicted load-displacement curves and shear stress distributions at the load level of 800 kN are shown in Fig. 9(a) and Fig. 9(b), respectively. In cases when grout strength is lower, tension stiffening is initiated sooner, resulting in higher predicted displacements and slightly lower ultimate bearing capacities due to the non-uniformity in shear stress distributions. Two points in Fig. 9(a) indicate the load levels at which initial grout cracking was initiated in calculations with f_t = 0.5 and 2 MPa.

5.1.6 Post-grouting, grout consolidation

Three analyzed alternatives are summarized in Table 2. In the first alternative, the post-grouting effect is not taken into account (*ID* 1). In the second (*ID* 2), radial stresses acting on the fixed length surface are updated utilizing the cylindrical cavity expansion theory (Randolph *et al.* (1979)). In the third (*ID* 3) calculation, the second alternative is complemented by a grout consolidation.

Table 2 Alternative calculations: post-grouting, grout consolidation

ID	Stress conditions	Grout consolidation
1	K_0 conditions	-
2	Randolph *et al.* (1979)	-
3	Randolph *et al.* (1979)	10%

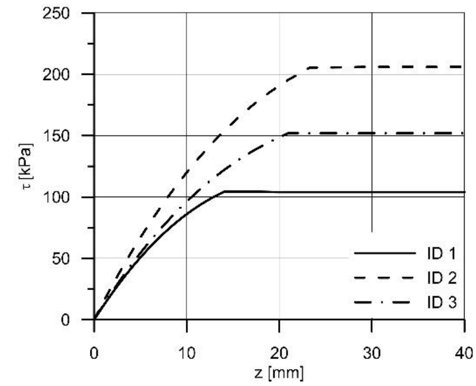

(a) Assembled load-transfer functions

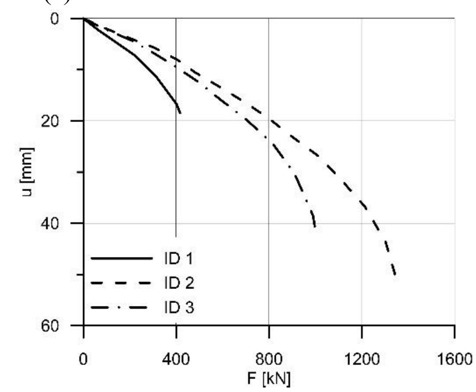

(b) Predicted load-displacement curves

Fig. 10 Influence of post-grouting and grout consolidation

Table 3 Predicted carrying capacities for various anchor fixed lengths

L_{fixed}	n_{seq}	F_{max}	F_{ult}	f_{eff}	L_{res}
[m]	[-]	[kN]	[kN]	[-]	[m]
6	15	740.8	677.8	0.91	1.0
8	20	987.7	822.3	0.83	1.8
10	30	1481.6	1069.6	0.72	6.2
12	50	2469.3	1563.2	0.63	14.2

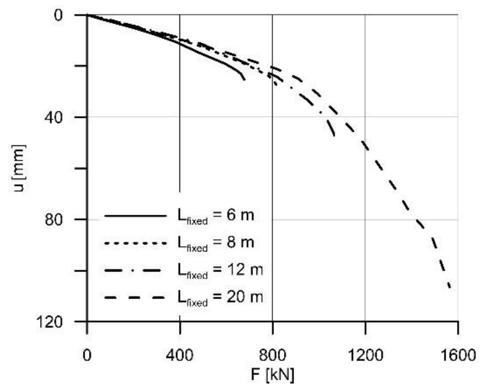

(a) Predicted load-displacement curves

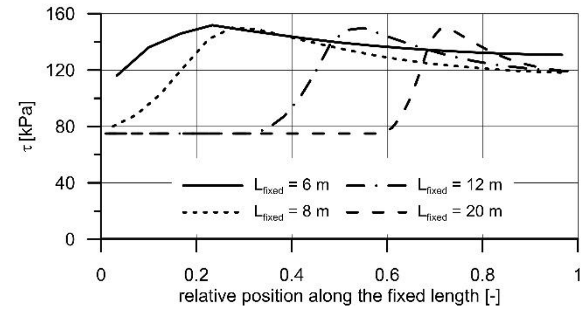

(b) Shear stress distributions in ultimate state

Fig. 11 Influence of anchor fixed length

The advantage of the proposed procedure is that the effect of post-grouting is incorporated directly into the load-transfer function assembly process (Fig. 10(a)). This means that the change in radial stress affects both the stiffness and the ultimate bond strength. For the sake of clarity, the post-failure segments are not considered in this study, the ultimate bond strength is held constant. The predicted load-displacement curves are shown in Fig. 10(b). Considering the post-grouting effect without grout consolidation, the predicted ultimate capacity was the highest of all alternatives. Combination with grout consolidation in the third calculation resulted in a decrease of the radial stress acting on the surface of the anchor fixed length. Lower shear strength of the grout-soil interface was therefore mobilized which was consequently reflected in the computed initial stiffness of the load-displacement curve and the ultimate carrying capacity.

5.1.7 Anchor fixed length

Finally, the input parameters from Table 1 are applied in the parametric study in which the anchor fixed length L_{fixed} is varied. The number of segments n_{seg} is chosen so as to keep the segment length l_{seg} constant (0.4 m). The predicted ultimate carrying capacities F_{ult} are summarized in Table 3. F_{max} is the theoretical carrying capacity assuming a uniform distribution of peak skin friction along the fixed length. The efficiency coefficient f_{eff} is evaluated as the ratio between F_{ult} and F_{max}, L_{res} indicates the portion of the fixed length in the critical stress state. Predicted load-displacement curves and shear stress distributions for ultimate load levels are shown in Fig. 11(a) and Fig. 11(b).

5.2 Verification

The responses of three ground anchors during investigation load tests at two different testing sites were predicted by the program. The basic geometrical characteristics of the anchors are summarized in Table 4. The anchors were constructed in similar geological conditions; their fixed lengths were situated in stiff Neogene clays with very high plasticity F8 CV (w = 33%, w_L = 77%, w_P = 30%). The case studies were undertaken as class C predictions according to Lambe (1973) (prediction after the event, but the results are not known at the time the prediction is made). The only information taken from results/construction logs a priori was related to post-

Table 4 Investigation anchor load tests analysed in case studies

Location	ID	Grouting	L_{free} [m]	L_{fixed} [m]
Holubice	K6	TAM*, 2 stages	8	8
Brno-Arboretum	II-B	TAM*, 1stage	5	8
	II-C1	TAM*, 1 stage	5	10

*TAM: Tube-A-Manchette grouting system

grouting and anchor geometry. These parameters are, however, prescribed by the design engineer in practice. The load-transfer curves were assembled assuming $R_f = 0.9$. The soil input parameters values were derived as follows:

- Variables K, n and ϕ_{cs} were from three CU triaxial tests (Svoboda *et al.* (2010)) with different effective confining pressures.
- Peak strength characteristics c_p and ϕ_p were from direct shear tests; the values are valid for a range of normal stress between 200 kPa and 400 kPa.
- The post-failure segment was assembled based on the direct shear stress with the effective normal stress of 200 kPa.

5.2.1 Case study I: Holubice

Prestressed ground anchors were constructed in the village of Holubice near the city of Brno in the Czech Republic. An investigation test conducted on the anchor with L_{fixed} = 8.0 m (Misove (1984)) was analyzed in this study. Apart from standard monitoring involving head displacements and prestressing forces, the fixed length tendon was equipped with electric resistance gauges. This made it possible to derive skin friction distributions for individual loading stages. Furthermore, the anchor was excavated after the test in order to measure the fixed length diameter (d_{fixed} = 263 mm). A comparison between the predicted and measured load-displacement curves is shown in Fig. 12. The measured head displacements at the load level of 100 kN (datum load) were zeroed during the test. In order to be able to compare both curves, the same action was undertaken for the predicted curve.

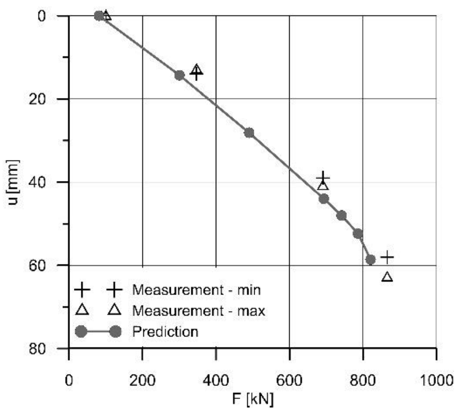

Fig. 12 Measured and predicted load-displacement curves: Case study I

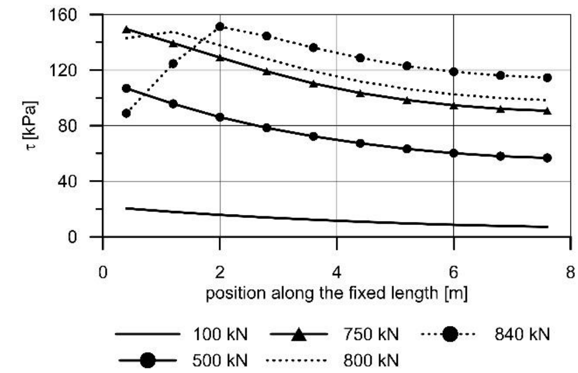

(a) Shear stress distributions

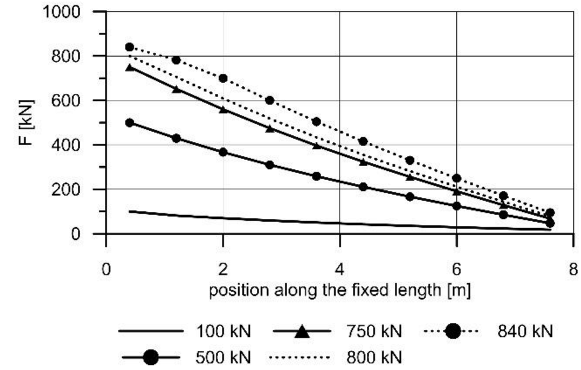

(b) Axial force distributions

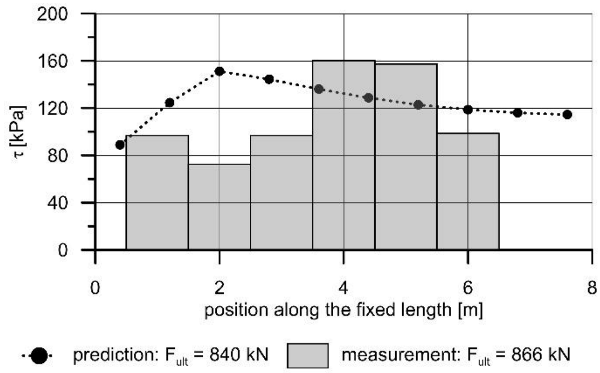

(c) Predicted and measured shear stress distributions in ultimate state

Fig. 13 Shear stress and axial force distributions: Case study I

The predicted ultimate carrying capacity is slightly lower than the measured one. Shear stress and axial force distributions along the fixed length are shown in Fig. 13(a) and Fig. 13(b). At the load level of 750 kN, the peak shear stress is mobilized at the closest end of the fixed length. When the load level increases, softening is triggered in the larger section of the fixed length. The ultimate state is reached when the decrease in stress due to softening is faster than its mobilization in more distant sections of the fixed length which are still in the hardening regime. Finally, the measured and predicted ultimate shear stress distributions are compared in Fig. 13(c). The measured shear stresses represent average values between measuring points (positions of electric resistance gauges) and therefore it was not possible to determine the shear stress profile

Table 5 Updated parameters in Case study II

Variable	II-B	II-C1
s_u [kPa]	135	145
d_{fixed} [mm]	232	250
V_i [l/valve]	8.5	12

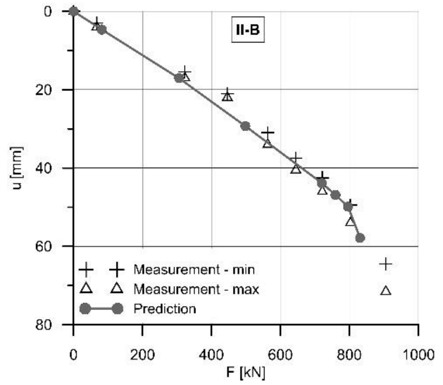

(a) Anchor n. II-B

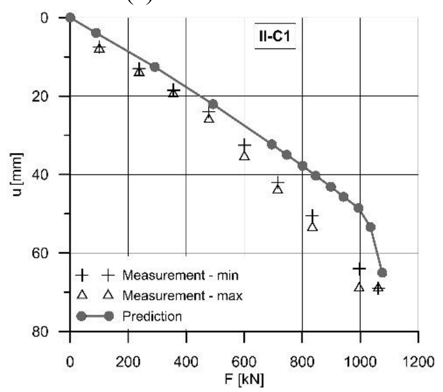

(b) Anchor n. II-C1

Fig. 14 Measured and predicted load-displacement curves: Case study II

more precisely. The predicted peak and critical bond strength match the corresponding experimental values reasonably well, but the peak bond strength locations differ by 1.5 meters. This might be due to the fact that a slightly higher ultimate force was obtained in reality. Consequently, softening was triggered on a longer section. The experimentally observed behavior also shows a higher softening rate compared to the prediction. Thus, a higher shear stress drop in the post-peak section of the anchor must be compensated by an additional shear strength mobilization in more distant sections of the anchor.

5.2.2 Case study II: Brno-Arboretum

Two anchors, II-B (L_{fixed} = 8.0 m) and II-C1 (L_{fixed} = 10.0 m), were analyzed. Both anchors were situated in similar geological conditions compared to the first case study. The load tests conducted at this location are part of a test site operated by the author's home institution. The variables that need to be modified are summarized in Table 5.

The predicted and measured load-displacement curves are shown in Fig. 14(a) and Fig. 14(b). A good match in terms of displacements is obtained for the II-B anchor. The

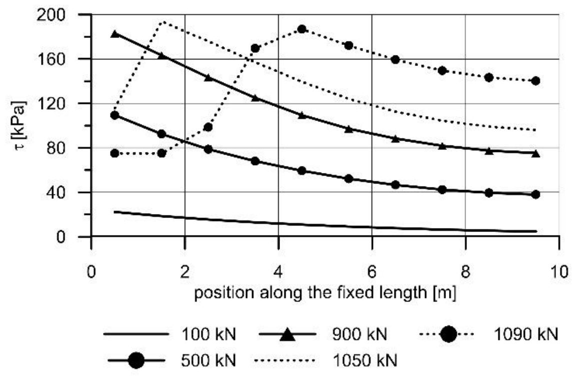

(a) Shear stress distributions

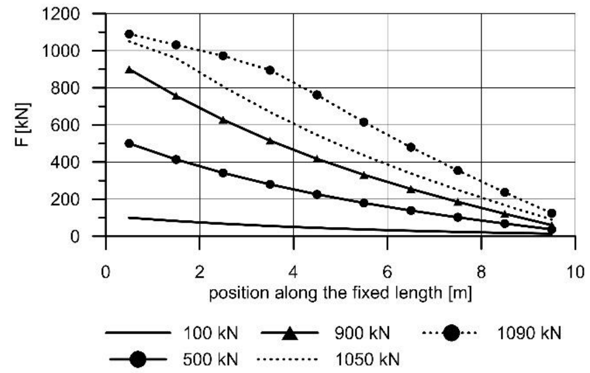

(b) Axial force distributions

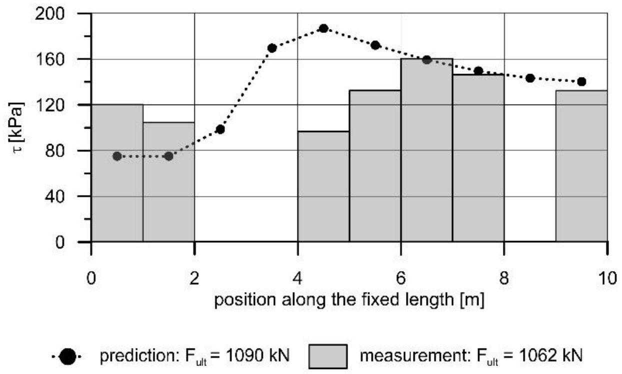

(c) Predicted and measured shear stress distributions in ultimate state

Fig. 15 Shear stress and axial force distributions: Case study II, anchor n. II-C1

ultimate force is slightly under-predicted. For anchor II-C1 the prediction yields a stiffer response, but the bearing capacity is predicted well. Further detailed results are presented for the anchor II-C1, which has a longer fixed-length (L_{fixed} = 10.0 m). Shear stress and axial force distributions are presented in Fig. 15(a) and Fig. 15(b). At a load level of 900 kN (86% of the ultimate carrying capacity), skin friction of less than 80 kPa (42% of the ultimate bond strength) is mobilized at the distant end. This only emphasizes the necessity of involving non-linear soil stress-strain behavior in anchor design. At the ultimate state (1050 kN), more than 4 m of the fixed length is in the post-failure regime. Finally, the shear stress distribution in the ultimate state is compared with the distribution derived from measurement by electric resistance gauges (Fig.

15(c)). Three gauges were probably damaged during the post-grouting of the anchor.

The non-linear shear stress distribution combined with the decrease in post-failure stress in the near section was observed. The predicted peak bond strength is 20 kPa larger than the measured one and their locations differ by 2 meters with the experimentally observed post-peak section longer than the predicted one. The assumed reason for this is that the real fixed length diameter of II-C1 anchor was smaller than the estimated one due to more grout losses during the post-grouting. This assumption is also supported by a fact that, compared to the calculation, lower overall axial stiffness and consequently higher anchor head displacements were observed during the loading test (Fig. 14(b)). The smaller surface area of the fixed length required a higher degree of shear stress mobilization for a given loading stage and thus a longer section of the fixed length reached the post-failure (softening) regime.

6. Conclusions

In this paper, an approach adopting the load-transfer method for the prediction of prestressed ground anchors performance is presented. The following conclusions are drawn:

- The non-linear strain-softening load-transfer function is utilized. Thus, the factors of non-constant skin friction distribution and progressive failure phenomena were involved in the analysis resulting in a reduction of an anchor efficiency with the increasing fixed length.
- In order to determine the radial stress acting on the soil-grout interface, the post-grouting process is modeled as the expansion of a cylindrical cavity followed by consolidation of the soil around the fixed length. Volume loss due to the grout consolidation must be also considered in order to assess the residual grouting pressure correctly.
- The compound axial stiffness, in which contributions of the tendon and surrounding grout are taken into account, does not remain constant but it decreases with increasing load level due to the occurrence of tensile cracks in the grout. The gradual stiffness reduction results in higher predicted displacements and less uniform shear stress profiles.
- The developed algorithm was verified in two case studies, in which three investigation anchor load tests were analyzed. In both studies, measurements by means of electric resistance gauges confirmed the occurrence of the post-failure shear stress drop. The performed analyses were able to simulate this behavior, though there were certain differences in the predicted locations of acting peak shear stress.

Acknowledgments

This research was supported by Ministry of Industry and Trade research project No. FR-TI4/329. The authors would also like to thank Ing. Peter Misove, CSc. (VUIS Special Foundations, Slovakia) for making his data and research available. Discussions with Dr. Vaclav Racansky (Keller Grundbau, Austria) are highly appreciated.

References

ACI 318-14 (2014), Building Code Requirements for Structural Concrete and Commentary, American Concrete Institute; Farmington Hills, Michigan, U.S.A.

Barley, A.D. (1997), "The single bore multiple anchor system", *Proceedings of the International Conference on Ground Anchorages and Anchored Structures*, London, U.K., March.

Bezuijen, A. and Talmon, A.M. (2006), *Grout Pressures around a Tunnel Lining, Influence of Grout Consolidation and Loading on Lining*, in *Tunnelling: A Decade of Progress*, 104-114.

Bohn, C., Dos-Santos, A.L. and Frank, R. (2017), "Development of axial pile load transfer curves based on instrumented load tests", *J. Geotech. Geoenviron. Eng.*, **143**(1), 04016081. https://doi.org/10.1061/(ASCE)GT.1943-5606.0001579.

Bustamante, M. and Diox, B. (1985), "Une méthode pour le calcul des tirants et des micropieux injectés", *Bull. Liaison LCPC*, **140**(3), 75-92.

CEB-FIP Model Code (1990), Design Code (1993), Comite Euro-International Du Beton.

Dias, T.G.S. and Bezuijen, A. (2017), "Load-transfer method for piles under axial loading and unloading", *J. Geotech. Geoenviron. Eng.*, **144**(1), 4017096. https://doi.org/10.1061/(ASCE)GT.1943-5606.0001808.

Duncan, J. and Chang, C. (1970), "Non-linear analysis of stress and strain in soils", *J. Soil Mech. Found. Div.*, **96**(5).

EN 1537 (2013), Execution of special geotechnical works. Ground anchors, European Committee for Standardization, Brussels, Belgium.

EN 1997-1 (2004), Eurocode 7 — Geotechnical design, Part 1: General rules, European Committee for Standardization, Brussels, Belgium.

Fabris, C., Schweiger, H. and Tschuchnigg, F. (2018), "Fe-analysis of anchor pull out tests using advanced constitutive models", *Proceedings of the 9th European Conference on Numerical Methods in Geotechnical Engineering (NUMGE2018)*, Porto, Portugal, June.

ISO 22477-5 (2018), Geotechnical Investigation and Testing — Testing of Geotechnical Structures — Part 5: Testing of Grouted Anchors, International Organization for Standardization (ISO), Geneva, Switzerland.

Kraft, L.M., Kagawa, T. and Ray, R.P. (1997), "Theoretical t-z curves", *J. Geotech. Eng. Div.*, **107**(11), 1543-1561.

Krammer, H. (1978), "Determination of the carrying capacity of ground anchors with the correlation and regression analysis", *Rev. Fr. Geotech.*, **3**, 76-81. https://doi.org/10.1051/geotech/1978003076.

Lambe, T.W. (1973), "Predictions in soil engineering", *Géotechnique*, **23**(2), 149-202. https://doi.org/10.1680/geot.1973.23.2.151.

Larsen, P. (2007), "Soil anchors in clay till using post-grouting", *Proceedings of the 14th European Conference on Soil Mechanics and Geotechnical Eng.*, Madrid, Spain, September.

Littlejohn, G.S. (1980), "Design estimation of the ultimate load-holding capacity of ground anchors", *Ground Eng.*, **13**(8), 25-39.

Misove, P. (1984), "Construction of prestressed ground anchors and their bearing capacity (in Slovak)", Ph.D. Dissertation, VUIS, Slovakia.

Monsberger, C., Woschitz, H., Lienhart, W., Račansky, V. and Hayden, M. (2017), "Performance assessment of geotechnical structural elements using distributed fiber optic sensing", *Proceedings of SPIE 10168: Smart Structures and NDE*, Portland, Oregon, U.S.A., March.

Mothersille, D., Duzceer, R., Gokalp, A. and Okumusoglu, B. (2015), "Support of 25 m deep excavation using ground anchors in Russia", *Geotech. Eng.*, **168**(GE4), 281-295. https://doi.org/10.1680/geng.14.00043.

Navratil, J. (2008), *Prestressed Concrete Structures*, CERM, Brno, Czech Republic (in Czech).

Ostermayer, H. (1975), "Construction carrying behaviour and creep characteristics of ground anchors", *Proceedings of the Conference of Diaphragm Walls and Anchorages*, London, U.K., September.

Pelecanos, L. and Soga, K. (2018), "Development of load-transfer curves for axially-loaded piles based on inverse analysis of fibre-optic strain data using finite element analysis and optimisation", *Proceedings of the 9th European Conference on Numerical Methods in Geotechnical Engineering (NUMGE2018)*, Porto, Portugal, June.

PTI (2004), *Recommendations for Prestressed Rock and Soil Anchors*, Post-Tensioning Institute, U.S.A.

Randolph, M.F. and Wroth, C.P. (1978), "Analysis of deformation of vertically loaded piles", *J. Geotech. Eng.*, **104**(12), 1465-1488.

Randolph, M.F., Steenfelt, J.S. and Wroth, C.P. (1979), "The effect of pile type on design parameters for driven piles", *Proceedings of the 7th European Conference on Soil Mechanics and Foundation Engineering*, Brighton, U.K., September.

Reddy, E.S.B., O'Reily, M. and Chapman, D.N. (1997), "A software to predict the behaviour of tension piles", *Comput. Struct.*, **62**(4), 653-658. https://doi.org/10.1016/S0045-7949(97)80002-3.

Reddy, E.S.B., O'Reily, M. and Chapman, D.N. (1998), "Modified T-Z model - a software for tension piles", *Comput. Struct.*, **68**(6), 613-625. https://doi.org/10.1016/S0045-7949(98)00089-3.

Seo, H.J. and Pelecanos, L. (2018), "Finite element analysis of soil-structure interaction in soil anchor pull-out tests", *Proceedings of the 9th European Conference on Numerical Methods in Geotechnical Engineering (NUMGE2018)*, Porto, Portugal, June.

Sulaiman, I.H. and Coyle, H.M. (1976), "Uplift resistance of piles in sand", *J. Geotech. Eng. Div.*, **102**(5), 559-562.

Svoboda, T., Masin, D. and Bohac, J. (2010), "Class A predictions of a NATM tunnel in stiff clay", *Comput. Geotech.*, **37**(6), 817-825. https://doi.org/10.1016/j.compgeo.2010.07.003.

Vukotic, G., Gonzalez Galindo, J. and Soriano A. (2013), "The influence of bond stress distribution on ground anchor fixed length design. Field results and proposal for design methodology", *Proceedings of the 18th International Conference on Soil Mechanics and Geotechnical Engineering*, Paris, France, September.

Weerasinghe, R.B. and Littlejohn, G.S. (1997), "Load transfer and failure of anchorages in weak mudstone", *Proceedings of the International Conference on Ground Anchorages and Anchored Structures*, London, U.K., March.

Woods, R.I. and Barkhordari, K. (1997), "The influence of bond stress distribution on ground anchor design", *Proceedings of the International Conference on Ground Anchorages and Anchored Structures*, London, U.K., March.

Wu, J., Cheng, Q., Wen, H., Wang, L., Li, Y. and Zhang J. (2016), "A load transfer approach to rectangular closed diaphragm walls", *Proc. Inst. Civ. Eng. Geotech. Eng.*, **169**(6), 509-526. https://doi.org/10.1680/jgeen.15.00156.

Wu, Y., Liu, J. and Chen, R. (2015), "An analytical analysis of a single axially-loaded pile using a nonlinear softening model", *Geomech. Eng.*, **8**(6), 769-781. https://doi.org/10.12989/gae.2015.8.6.769.

Zhang, Q., Li, S., Liang, F., Yang, M. and Zhang, Q. (2014), "Simplified method for settlement prediction of single pile and pile group using a hyperbolic model", *Int. J. Civ. Eng.*, **12**(2), 146-159.

Zou, J.F., Yang, T. and Deng, D. (2019), "Field test of the long-term settlement for the post-grouted pile in the deep-thick soft soil", *Geomech. Eng.*, **19**(2), 115-126. https://doi.org/10.12989/gae.2019.19.2.115.

CC